



TITLE:

# N-glycosylation enables high lateral mobility of GPI-anchored proteins at a molecular crowding threshold

AUTHOR(S):

Hartel, Andreas J. W.; Glogger, Marius; Jones, Nicola G.;  
Abuillan, Wasim; Batram, Christopher; Hermann, Anne;  
Fenz, Susanne F.; Tanaka, Motomu; Engstler, Markus

---

CITATION:

Hartel, Andreas J. W. ...[et al]. N-glycosylation enables high lateral mobility of GPI-anchored proteins at a molecular crowding threshold. Nature Communications 2016, 7: 12870.

ISSUE DATE:

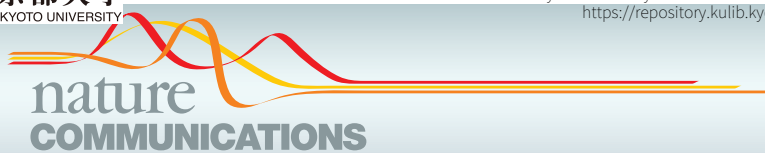
2016-09-19

URL:

<http://hdl.handle.net/2433/235332>

RIGHT:

© The Author(s) 2016. This work is licensed under a Creative Commons Attribution 4.0 International License. The images or other third party material in this article are included in the article's Creative Commons license, unless indicated otherwise in the credit line; if the material is not included under the Creative Commons license, users will need to obtain permission from the license holder to reproduce the material. To view a copy of this license, visit <http://creativecommons.org/licenses/by/4.0/>



## ARTICLE

Received 31 May 2016 | Accepted 9 Aug 2016 | Published 19 Sep 2016

DOI: 10.1038/ncomms12870

OPEN

# N-glycosylation enables high lateral mobility of GPI-anchored proteins at a molecular crowding threshold

Andreas J.W. Hartel<sup>1,\*†</sup>, Marius Glogger<sup>1,\*</sup>, Nicola G. Jones<sup>1,\*\*</sup>, Wasim Abuillan<sup>2</sup>, Christopher Batram<sup>1</sup>, Anne Hermann<sup>1</sup>, Susanne F. Fenz<sup>1,\*\*</sup>, Motomu Tanaka<sup>2,3,\*\*</sup> & Markus Engstler<sup>1,\*\*</sup>

The protein density in biological membranes can be extraordinarily high, but the impact of molecular crowding on the diffusion of membrane proteins has not been studied systematically in a natural system. The diversity of the membrane proteome of most cells may preclude systematic studies. African trypanosomes, however, feature a uniform surface coat that is dominated by a single type of variant surface glycoprotein (VSG). Here we study the density-dependence of the diffusion of different glycosylphosphatidylinositol-anchored VSG-types on living cells and in artificial membranes. Our results suggest that a specific molecular crowding threshold (MCT) limits diffusion and hence affects protein function. Obstacles in the form of heterologous proteins compromise the diffusion coefficient and the MCT. The trypanosome VSG-coat operates very close to its MCT. Importantly, our experiments show that N-linked glycans act as molecular insulators that reduce retarding intermolecular interactions allowing membrane proteins to function correctly even when densely packed.

<sup>1</sup>Department of Cell and Developmental Biology, Theodor-Boveri-Institute, Biocenter, University of Würzburg, Würzburg 97074, Germany. <sup>2</sup>Physical Chemistry of Biosystems, Institute of Physical Chemistry, University of Heidelberg, Heidelberg 69120, Germany. <sup>3</sup>Institute for Integrated Cell-Material Science (WPI iCeMS), Kyoto University, Kyoto 606-8501, Japan. \* These authors contributed equally to this work. \*\* These authors jointly supervised this work. † Present address: Department of Electrical Engineering, Bioelectronic Systems Lab, Columbia University, New York, New York 10027, USA. Correspondence and requests for materials should be addressed to M.E. (email: markus.engstler@biozentrum.uni-wuerzburg.de).

**B**iological membranes are vital components of all living systems, as they form the outer boundary of cells and enclose their internal compartments. They consist of a lipid bilayer that imparts a fluid character, and a multitude of membrane-associated proteins with a range of functions.

The translational diffusion of proteins in biological membranes has been described theoretically by Saffman and Delbrück within the framework of a continuum approach<sup>1</sup>. In their landmark model, the diffusion coefficient of a particle embedded in a membrane is largely determined by the viscosity and thickness of the bilayer and has only a weak dependence on the radius of the membrane-spanning domains. The translational diffusion coefficient of a cylindrical particle (radius  $R_p \ll h$ ,  $\mu_m/\mu_w$ ) immersed in a quasi-two-dimensional (2D) continuum bounded by less viscous medium ( $\mu_w \ll \mu_m$ ) is

$$D = \frac{k_B T}{4\pi\mu_m h} \ln\left(\frac{\mu_m h}{\mu_w R_p} - \gamma\right), \quad (1)$$

where  $k_B$  is the Boltzmann constant,  $T$  the temperature,  $\mu_w$  and  $\mu_m$  are the bulk viscosities of the surrounding medium and the lipid membrane, respectively. The height of the particle  $h$  equals the thickness of the bilayer, and  $\gamma$  is the Euler's constant ( $\gamma = 0.5772$ ). The Saffman–Delbrück (SD) model was verified experimentally for protein and peptide diffusion in model membranes<sup>2–7</sup>. A more general, but mathematically more complex model, valid for arbitrary viscosities of the membrane and surrounding medium as well as a larger range of  $R_p$ , was provided by Hughes *et al.*<sup>8</sup> Today, a reliable analytical approximation of this model is available thus facilitating its use<sup>9</sup>.

To model the lateral diffusion of lipids and proteins in contact with asymmetric environments, such as a rigid substrate, Evans and Sackmann extended the continuum model by taking asymmetric boundary conditions and the resulting friction on the membrane into account<sup>10</sup>.

The above models are based on the assumption that sparsely dispersed proteins undergo free random walks and therefore do not account for the potentially high protein density on biological membranes<sup>11</sup>. Other theoretical studies have considered higher surface densities. They predict that the lateral diffusion of a given protein is hindered by the presence of additional proteins, which act as obstacles<sup>12–14</sup>. Experiments both in crowded model membranes<sup>5,15–17</sup> and living cells<sup>18,19</sup> reported reduced normal diffusion, emergence of sub-diffusion, obstructed diffusion or clustering as a function of protein density.

Coarse-grained molecular dynamics simulations in crowded membranes predicted sub-diffusion on the microsecond timescale and reduced diffusion at experimentally accessible scales<sup>20–22</sup>. Recently, a study based on dissipative particle dynamics suggested a relation between the friction coefficient introduced by crowding and the diffusion constant. In this model for dilute and semi-dilute conditions (occupied area fraction  $< 0.4$ ) the contribution of the total protein density to the friction coefficient is a polynomial of second order<sup>23</sup>.

The SD model and the subsequent mathematical calculations only take into account the membrane-spanning domain of a protein. The protein part that protrudes above the membrane is deemed to have no effect on diffusion, since the viscosity of the surrounding medium is much lower than the viscosity of the lipid bilayer. However, we and others could show that changes in the extra-membrane domain of a protein significantly changes the resulting diffusion coefficient<sup>24–27</sup>. In this work, we address another parameter that cannot be captured by these simple models: the effect of molecular crowding in the semi-dilute approximation and beyond, which has so far not been studied in a natural system.

This may be due to the fact that the vast majority of cells exhibit a great diversity of membrane proteins, each of varying abundance and with different properties. The sizes of the various proteins differ, as do the mode and degree of membrane attachment. Thus, a natural cell system with reduced complexity, high flexibility, yet maximum conservation is required to assess the potential impact of molecular crowding on biological membranes in a comparative and quantitative manner. We suggest that the surface coat of African trypanosomes, the causative agents of sleeping sickness in humans and Nagana in cattle, provides such a model. The unicellular parasites are covered with a dense layer of variant surface glycoproteins (VSGs). About 95% of all surface proteins are VSGs<sup>28</sup>. An extracellular matrix does not exist<sup>29</sup>. There is strong selective pressure for the VSG coat to maintain a sufficiently high density, as it functions in shielding other membrane proteins from recognition by the host's immune system<sup>30</sup>. African trypanosomes possess several hundred different VSG genes, of which only one is expressed at any given time. Random switches to the expression of a new VSG allow escape from the mammalian immune response by antigenic variation<sup>31</sup>. Thus, there is selective pressure for a VSG repertoire that is not only diverse in sequence but also shows structural conservation. Although VSGs are thought to be structurally similar<sup>32,33</sup>, they are immunologically clearly distinct. In addition, VSGs are glycosylphosphatidylinositol (GPI)-anchored proteins<sup>34</sup>, which means they are attached only to the outer leaflet of the plasma membrane by the GPI moiety. As a consequence, the interaction between the proteinaceous part and the plasma membrane is minimized when compared with transmembrane domains. Since the core structure of the membrane anchor of all VSG types is identical<sup>35</sup>, true comparative studies to elucidate the role of the free protein part on diffusion become possible.

Here we present a systematic study on the influence of protein lateral density and N-glycosylation on the diffusion of the GPI-anchored VSG first on the trypanosome cell surface, and second in a more defined artificial supported membrane system. Our data indicate the presence of a molecular crowding threshold (MCT) for lateral diffusion. The MCT is not only determined by the lateral protein density but also by the biochemical properties of the proteins. We found that the trypanosome cell surface acts remarkably close to its MCT. This threshold is modulated by N-glycosylation.

## Results

**The diffusion behaviour of different VSGs is comparable.** We established both an *in vivo* and an *in vitro* experimental system for direct comparison of the diffusion of VSGs in natural and artificial surface coats. First, we developed a straightforward method to immobilize the motile flagellate parasites<sup>36</sup>. Cells were incubated in a custom-made observation chamber in trypanosome dilution buffer (TDB) or PBS, containing ~6% (w/v) type A gelatin. At 37 °C, this solution is fluid, allowing normal cellular movement. With decreasing temperature the gelatin becomes solid, resulting in complete immobilization of trypanosomes at 20 °C. It should be noted that this process is fully reversible and allows immobilization of various trypanosome strains and species for several hours without any negative impact on subsequent growth of the trypanosomes after their release from the solid matrix (Supplementary Note 1 and Supplementary Fig. 1).

Although it appears common knowledge that the diffusion of different VSGs (MW = 50–60 kDa per monomer) is similar, no comparative measurements have been reported to date. The diffusion constant for one VSG has, however, been determined<sup>37</sup>. Therefore, the diffusion coefficients and mobile fractions of a variety of fluorescently labelled VSGs were determined on living

**Table 1 | Diffusion of various VSGs on live cells and on supported membranes.**

Live cells				Supported membranes			
VSG (no. of N-Glycans)	Diffusion coefficient ± s.d. (μm <sup>2</sup> s <sup>-1</sup> )	Mobile fraction ± s.d. (%)	N	VSG (no. of N-Glycans)	Diffusion coefficient ± s.d. (μm <sup>2</sup> s <sup>-1</sup> )	Mobile fraction ± s.d. (%)	N
121 WT (1)	0.024 ± 0.010	79 ± 9	110	121 WT (1)	1.0 ± 0.3	94 ± 6	61
121 MUT (0)	0.021 ± 0.010	71 ± 7	56	121 MUT(0)	0.7 ± 0.2	95 ± 8	56
117 WT (1)	0.028 ± 0.009	80 ± 6	43				
117 MUT (0)	0.030 ± 0.013	75 ± 6	36				
060 (2)	0.021 ± 0.013	74 ± 7	40	060 (2)	0.9 ± 0.2	94 ± 5	41
221 (2)	0.021 ± 0.008	76 ± 6	28	221 (2)	0.7 ± 0.2	94 ± 8	58
118 (3)	0.027 ± 0.008	78 ± 8	25	118 (3)	0.7 ± 0.2	97 ± 2	41

VSG, variant surface glycoprotein.

cells by fluorescence recovery after photobleaching (FRAP) measurements. This experiment involved five trypanosome strains, expressing representative VSGs, which contain either one, two or three N-glycans<sup>38</sup>. The diffusion coefficients were found to lie within a narrow range, between 0.02 and 0.03 μm<sup>2</sup> s<sup>-1</sup>. The mobile fractions were ~80%, indicating that a very high fraction of VSGs moved freely on living trypanosomes (Table 1). This shows that despite marked differences in protein primary structure, domain architecture and number of N-glycans, the VGSs in fact display very similar diffusion parameters. Note, that the immobile fraction is only immobile on the timescales used for the experiment not, however, on longer timescales. In the next experiment, we compared the results obtained from living trypanosomes with purified VSGs inserted into artificial supported membranes. For protein isolation, we adopted a protocol that uses trifluoroacetic acid extraction and reversed-phase high-performance liquid chromatography<sup>39</sup>. Four types of purified mfVSGs were fluorescently labelled using succinimidyl ester chemistry and incorporated into preformed lipid bilayers, which were made by spreading small unilamellar lipid vesicles onto glass substrates. Equal amounts of different mfVSGs were allowed to incorporate into the lipid bilayers by incubation under standardized conditions. The diffusion coefficients determined for the different VSGs in the supported membranes were virtually identical (Table 1), which is in good agreement with the *in vivo* analysis. Furthermore, the diffusion coefficients of around 1.0 μm<sup>2</sup> s<sup>-1</sup> are comparable to those published for other GPI-anchored proteins in artificial lipid bilayers<sup>40</sup>, which emphasizes that VSGs are representative, model GPI-anchored proteins.

The diffusion coefficient of VSGs in supported membranes was significantly larger than on living trypanosomes. Several factors might be responsible, for example molecular crowding of VSG, the presence of heterologous proteins on the trypanosome cell surface, the differences in the lipid composition of the model and natural membrane, or high extracellular viscosity originating from gelatin embedding. The latter was ruled out by measuring the diffusion coefficients of VSG in supported membranes in the presence and absence of 6% (w/v) gelatin; no negative effect on the diffusion of VSG was observed (Supplementary Table 1). Therefore, we investigated the other feasible possibilities in separate sets of experiments.

**VSG coats operate close to a molecular crowding threshold.** We developed a system that allows precise adjustment of VSG density within supported membranes. The aim was to perform a direct comparison of the concentration of the proteins in artificial lipid bilayers with that on living trypanosomes. The exact number of cells in exponentially growing trypanosome cultures was determined by a linear dilution series and the corresponding amount of VSG was measured by immuno-detection and near infrared fluorescence scanning of dot blots. Next, we quantified the

amount of VSG incorporated into solid supported lipid bilayers after fusion of proteoliposomes to lipid monolayers, which had been prepared using a Langmuir film balance (see ‘Methods’ section for more details). Figure 1 shows the diffusion of VSGs at various lateral densities. Remarkably, the experiments revealed that a very high and controllable degree of molecular crowding could be achieved on artificial membranes. At and below protein concentrations corresponding to those found in the trypanosome surface coat, the diffusion coefficient of VSG is around 1.10 ± 0.20 μm<sup>2</sup> s<sup>-1</sup> (SD, N ≥ 21 for all data points). Upon further increase in VSG concentration, the diffusion coefficient decreased significantly to 0.10 ± 0.09 μm<sup>2</sup> s<sup>-1</sup> (SD, N = 24) and the mobile fraction dropped below 40%. Thus, there exists a critical value that limits VSG mobility that is a prerequisite for VSG functionality. We have termed this the MCT. The MCT of VSG was reached at 1.5-fold of the VSG concentration on living trypanosomes (Fig. 1a,b). This result was confirmed with a second complete set of experiments (Supplementary Fig. 2A,B).

In accordance with the model of Evans and Sackmann, we used the measured drop in the VSG diffusion constant to calculate the viscosity of the dense VSG protein layer μ<sub>VSG</sub> (see ‘Methods’ section). We found μ<sub>VSG</sub> ≈ 75 Pas, which is more than two orders of magnitude higher than the bulk viscosity of the artificial membrane. This result underpins the need for a new model describing diffusion of GPI-anchored proteins in dense environments such as the VSG coat or the extracellular matrix, where the popular SD model in the limit of μ<sub>w</sub> ≪ μ<sub>m</sub> cannot be applied anymore.

Our findings clearly indicate that the trypanosome VSG coat operates rather close to its MCT. Nevertheless, this threshold is above the concentration of VSG on the trypanosome cell surface. Does this mean that the plasma membrane of trypanosomes could actually harbour more VSG molecules? It would indeed appear sensible for the parasites to be able to transiently adjust VSG density, for example in the course of antigenic variation, when two VSGs populate the cell surface at the same time. In fact, ectopic VSG overexpression transiently raises the overall amount of VSG to roughly 140% of wild-type levels. This resembles the MCT measured *in vitro* and FRAP measurements showed that the diffusion coefficient of VSGs on living parasites is significantly reduced (*P* = 0.005, two-tailed and unpaired *t*-test) in the presence of excess VSG (Table 2). Thus, molecular crowding greatly influences VSG diffusion in artificial membranes and on living cells.

**Non-VSG proteins alter the crowding behaviour of the VSG.** In contrast to the artificial VSG coats described above, the cell surface of living parasites features at least 5% of non-VSG proteins. Little is known about the nature of these additional proteins or their exact distribution on the trypanosome cell surface and, hence, it is impossible to measure or even adjust the amount of invariant proteins in *in vivo* experiments. We therefore developed a straightforward strategy to study the potential

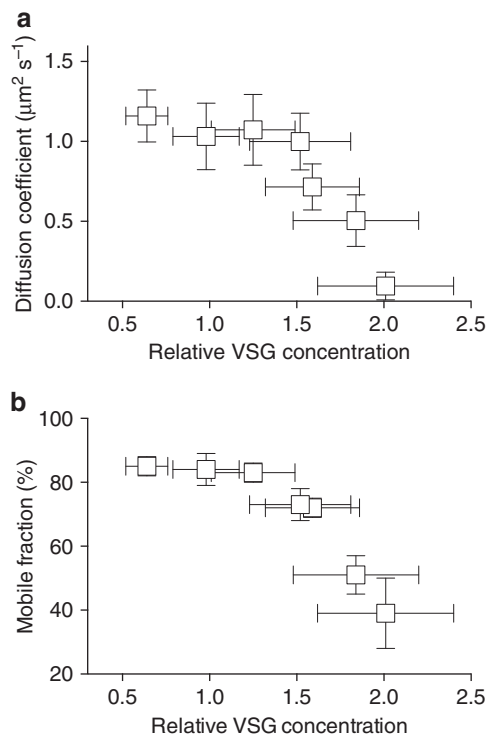


**Figure 1 | The VSG coat operates close to its MCT.** The impact of lateral protein density on the diffusion of VSG was quantified in supported membranes. Diffusion coefficients (**a**) and mobile fractions (**b**) are displayed as a function of the VSG concentration in relation to the concentration on the trypanosome cell surface. A relative concentration of 1 corresponds to the concentration *in vivo*. The error bars in y (diffusion coefficient) represent the standard deviation of the mean, while the error bars in x (relative VSG concentration) depict the range.

Table 2   Effect of VSG overexpression on the diffusion of VSG on live cells.			
Relative degree of VSG overexpression	Diffusion coefficient ± s.d. (μm² s⁻¹)	Mobile fraction ± s.d. (%)	N
1	0.020 ± 0.005	78 ± 11	18
1.2	0.019 ± 0.008*	79 ± 11	28
1.4	0.016 ± 0.005#	77 ± 11	29

VSG, variant surface glycoprotein.  
P value of the diffusion coefficients of a two-tailed and unpaired t-test compared with a degree of overexpression of 1: P\* > 0.03, P# = 0.005

influence of heterologous proteins on VSG diffusion using the supported membrane system. Lipid bilayers with varying concentrations of biotinylated phospholipids (DOPE-biotin) were generated. The diffusion of VSG in doped and non-manipulated supported membranes was virtually identical, which excludes a changed diffusion behaviour due to the membrane lipid composition. The presence of non-VSG proteins was simulated by addition of NeutrAvidin, a small protein (MW = 60 kDa) that strongly binds biotin. Strikingly, even comparatively small amounts of NeutrAvidin had a marked effect on VSG diffusion. Concentrations between 0.05 and 1 mol% DOPE-biotin reduced the diffusion coefficient of VSG to about one quarter of that observed in the absence of DOPE-biotin without having a comparable effect on the mobile fraction, which was only reduced from 90% to 75% (Fig. 2). When DOPE-biotin was added

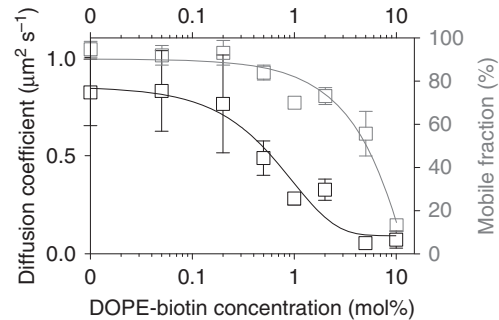


**Figure 2 | Influence of varying concentrations of membrane-bound NeutrAvidin on the diffusion of VSG in supported membranes.** The black squares indicate VSG diffusion coefficients and grey squares represent the corresponding mobile fractions. Trend lines are inserted as a guide for the reader's eye. At high concentrations of non-VSG proteins (5–10% DOPE-biotin) the diffusion coefficients decrease more than 15-fold and VSG mobility is reduced to 20%. At low concentrations of non-VSG (0.1–1% DOPE-biotin) the diffusion coefficients are decreased fourfold, whereas the mobile fraction is reduced to 70%. Data are presented as means ± s.d.

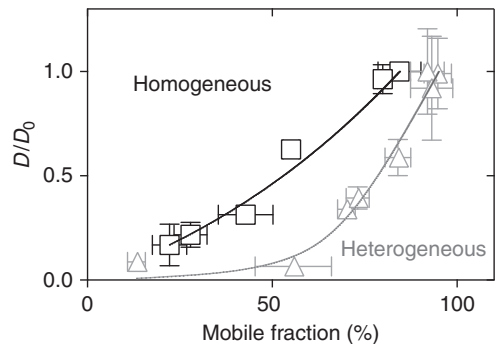


**Figure 3 | VSG diffusion depends on the density and homogeneity of the protein layer.** Comparison of the diffusion coefficients and the corresponding mobile fractions in homogenous VSG (black squares) and VSG/NeutrAvidin layers (grey triangles, cf. Fig. 2). Diffusion coefficients (*D*) are normalized to the values for the most dilute situation (*D*<sub>0</sub>). The solid lines represent the fit according to equation (6). Data are presented as means ± s.d.

in saturating amounts, the calculated frictional coefficients *b*<sub>s</sub> (see equations (3) and (4)) on VSGs before and after the addition of NeutrAvidin are *b*<sub>s, before</sub> = 4 × 10<sup>7</sup> N s m<sup>−3</sup> and *b*<sub>s, after</sub> = 8 × 10<sup>9</sup> N s m<sup>−3</sup>, respectively. Thus, the occupation of free area with NeutrAvidin results in a significant increase in the frictional stress experienced by the VSG proteins.

By contrast, in a homogenous VSG-layer, that is, in the absence of NeutrAvidin, an equivalent reduction of the diffusion coefficient was accompanied by a decrease of the mobile fraction to 30% (Fig. 3). This is an interesting result, as it indicates that non-VSG proteins can exert a smaller effect on VSG mobility than the VSG itself. Thus, the MCT not only depends on the concentration but also on the physicochemical nature of the crowding agents. How does this translate to the *in vivo* situation? The range of concentrations of NeutrAvidin used in our experiments is comparable to the 5–10% of non-VSG proteins on the trypanosome cell surface. The NeutrAvidin-bound DOPE is smaller than VSG and its diffusion coefficient is three-fourth of that of the VSG. This could also hold true for invariant proteins on the trypanosome surface. These proteins are shielded by the surface coat and hence, should generally be smaller than a VSG. Furthermore, many invariant proteins are transmembrane



proteins, which diffuse more slowly than GPI-anchored proteins<sup>41</sup>. Thus, the VSG/NeutrAvidin system emulates the parasite's surface coat with a good experimental accessibility, albeit with strongly reduced complexity. The fit of the data in Fig. 3 with equation (6) implies distinctly different  $\gamma$  values; in the presence of NeutrAvidin  $\gamma_{\text{inhom}} = 14 \pm 8$  and VSG alone  $\gamma_{\text{hom}} = 0.5 \pm 0.5$ . This finding suggests that the NeutrAvidin molecules do indeed hinder the diffusion of VSGs and may explain why the diffusion coefficient of the VSG on living trypanosomes was found to be smaller than on homogenous, supported membranes: on living cells the non-VSG proteins slow down VSG diffusion, as they act as obstacles in the crowded environment of the VSG coat. Importantly, while those obstacles impair the diffusion coefficient, the overall fraction of VSGs that is mobile remains largely unaffected. This physical property of the VSG coat could prove to be critical for trypanosome survival in the mammalian bloodstream. The parasites remove VSG-bound host antibodies with the help of hydrodynamic drag forces that are generated on the cell surface by directional cellular movement. The hydrodynamic flow pushes antibody-bound

VSGs against the swimming direction towards the flagellar pocket, where they are endocytosed and cleared from the circulation<sup>42</sup>. Since this hydrodynamic mechanism exerts an external force specifically on VSG-antibody complexes, the diffusion coefficient of the VSG is irrelevant, whereas the mobile fraction on the other hand becomes highly important. If VSG mobility were stalled, antibody clearance would lose its efficiency and the parasite its virulence.

**N-linked glycans facilitate membrane protein mobility.** Nearly all VSGs that have been proven to be functionally intact are modified by post-translational addition of N-linked glycans. To test the possibility that N-glycosylation modulates VSG diffusion, we have removed the N-glycosylation sites of two VSGs by site directed mutagenesis. The transgenic cell lines produced an N-glycan free surface coat without any changes in cell morphology or growth (Jones *et al.*, in preparation). While the diffusion coefficients of the VSG mutants were comparable to those of the respective wild-type proteins under *in vivo* conditions, their mobile fractions were significantly smaller

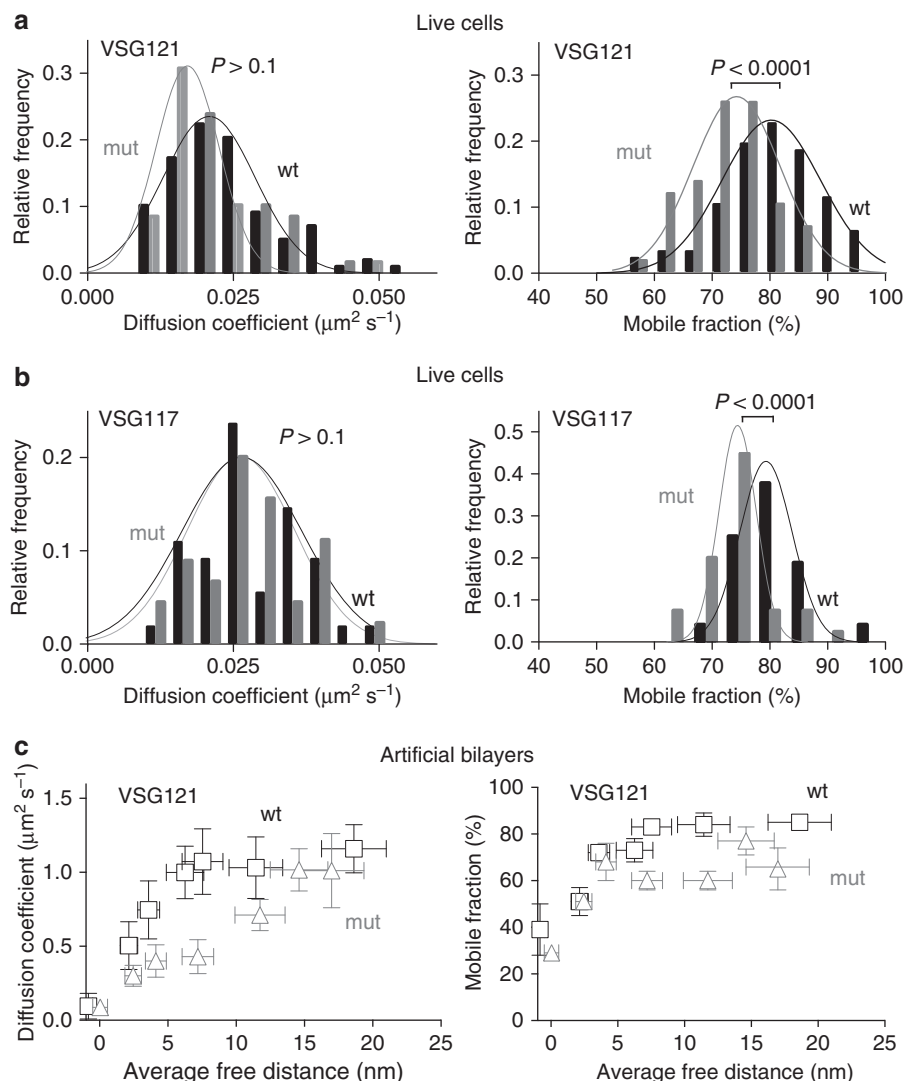


**Figure 4 | Impact of N-glycosylation on the diffusion of VSG.** The relative frequency distributions for wild-type (wt) and N-glycosylation deficient (mut) VSG121 (a) and VSG117 (b). Frequency distributions were fitted with a Gaussian function. The diffusion coefficients do not differ significantly, whereas there is a significant change in the mobile fractions of the wt and mut VSG. (c) Impact of the lateral protein density of wt and N-glycosylation deficient (mut) VSG121 on their diffusion in artificial membranes. The error bars in y (diffusion coefficient) represent the standard deviation of the mean, while the error bars in x (average free distance) depict the range. *P* values determined by an unpaired *t*-test.

(Fig. 4a,b). This means that N-glycosylation contributes to preserving high VSG mobility within the surface coat of living trypanosomes. Interestingly, both the diffusion coefficients of the mutant VSGs and their respective mobile fractions were reduced in the defined supported membranes system (Fig. 4c and Supplementary Fig. 2C,D). As a consequence of the lack of N-glycosylation, the MCT was shifted dramatically. VSG121 (wt) shows a MCT of between 5 and 7 nm average free protein distance, whereas the diffusion coefficient of its N-glycosylation mutant already begins to drop at larger distances ( $\sim 15$  nm). The mobile fractions decrease to 30–40% with increasing protein density. Further, an additional set of experiments, wherein the concentration in the VSG layers was again quantified in means of cell surface equivalents, shows that the MCT of the N-glycosylation deficient mutant VSG is already reached at a onefold concentration (Supplementary Fig. 3).

To probe *in vitro* VSG diffusion on time- and length scales beyond the resolution of the FRAP technique (1 min and 1  $\mu$ m, respectively), complementary single-molecule tracking experiments were implemented. To this end, the same SLBs as used in the FRAP measurements were further doped with trace amounts of VSG-ATTO 647N for single-molecule tracking on the millisecond timescale at a positional accuracy of  $20 \pm 12$  nm (SD,  $N > 1.2 \times 10^6$  localizations). For each condition a minimum number of 200 traces with a weighted mean trace length of 70 positions were analysed. Ensemble averaging allowed comparison with the FRAP results and yielded good agreement (see Fig. 5a,b). Close inspection of the individual traces revealed that the mobile

fraction was  $>90\%$  and independent of the VSG density throughout the phase space under investigation. However, as the coat densified an increasing fraction of the tracked VSGs exhibited confined diffusion in compartments well below the resolution limit of the FRAP technique (see Supplementary Fig. 4 for exemplary traces of free, confined and immobile VSGs). This fraction was generally larger for the mutant VSGs.

Therefore, we conclude, that N-glycosylation facilitates the dense packaging of VSG in 2D, probably by functioning as a structural ‘insulator’ that decreases, for example, attractive interactions as suggested by Høiberg-Nielsen *et al.*<sup>43</sup> for the three-dimensional situation. The ‘buffering’ property of N-glycans could be essential during antigenic variation and the microevolution of new mosaic VSGs.

In conclusion, the above experiments prove that the part of the protein protruding from the membrane significantly influences diffusion and lateral mobility of GPI-anchored proteins. We suggest that for each membrane protein, a specific MCT exists that limits diffusion and hence influences protein function. This goes beyond the theoretical considerations of Saffman and Delbrück. The MCT describes that point at which the protein density increases the viscosity of the proteinaceous layer on the membrane beyond a critical value where diffusion is affected. This viscosity is certainly higher than that of water and thus contributes substantially to the lateral diffusion of membrane-anchored proteins. The cell surface coat of African trypanosomes operates surprisingly close to its MCT, with N-glycosylation of the VSG playing a major role.

Because of its greatly reduced complexity, the trypanosome system appears ideal for comparative studies on membrane protein diffusion. Furthermore, the finding that N-glycosylation influences the MCT of VSG diffusion might pave the way for new therapies against the deadly sleeping sickness. Any interference with the MCT of the VSG coat would unequivocally kill the parasites. This time the drug target would not be a particular protein or process, but the entire cell surface; it is hard to envisage how resistance against such a prospective drug could arise.

## Methods

Additional information is provided in Supplementary Methods section.

**Trypanosomes.** *Trypanosoma brucei* bloodstream form (BSF) strains expressing VSG117, VSG121, VSG060, VSG221 or VSG118 were employed. N-glycosylation deletion mutants were generated based on the transgenic cell line 13-90 (ref. 44) by insertion of a mutated VSG121 or VSG117 coding sequence into the active VSG221 expression site via the construct pKD4 (ref. 45). Subsequently, the endogenous VSG221 gene was knocked out.

**Standard cultivation.** *T. brucei* BSF were cultivated in HMI-9 medium, supplemented with 10% fetal calf serum, at 37 °C and 5% CO<sub>2</sub>. Unless otherwise stated, the maximum cell density was limited to  $5 \times 10^5$  cells per ml.

**Cell surface staining.** A total of  $10^7$  trypanosomes were washed three times in ice-cold TDB (5 mM KCl, 80 mM NaCl, 1 mM MgSO<sub>4</sub>, 20 mM Na<sub>2</sub>HPO<sub>4</sub>, 2 mM NaH<sub>2</sub>PO<sub>4</sub>, 20 mM glucose, pH 7.6), trypanosome density was adjusted to  $1 \times 10^8$  cells per ml, and cells were incubated with 10  $\mu$ M ATTO 488 NHS-ester (ATTO-TEC GmbH, Siegen) for 15 min on ice in the dark. To remove unbound dye, the cells were washed three times with ice-cold TDB<sup>46</sup>.

**Immobilization of trypanosomes.** A total of  $10^7$  fluorescently labelled trypanosomes were suspended in 20  $\mu$ l of TDB. For immobilization 3  $\mu$ l of the cell suspension were added to 5  $\mu$ l of 10% (w/v) type A gelatin (from porcine skin; Sigma-Aldrich, Steinheim) in PBS, pH 7.8, warmed to 37 °C. The trypanosome-gelatin mixture was pipetted between two cover slips and mounted in a temperature-controlled sample holder, which was then cooled to 20 °C.

**High-density cultivation of trypanosomes.** Cells were grown to a cell density of  $8 \times 10^5$  cells per ml; then one volume of fresh HMI-9 medium, supplemented with 30% fetal calf serum, was added and incubation was continued in conical glass

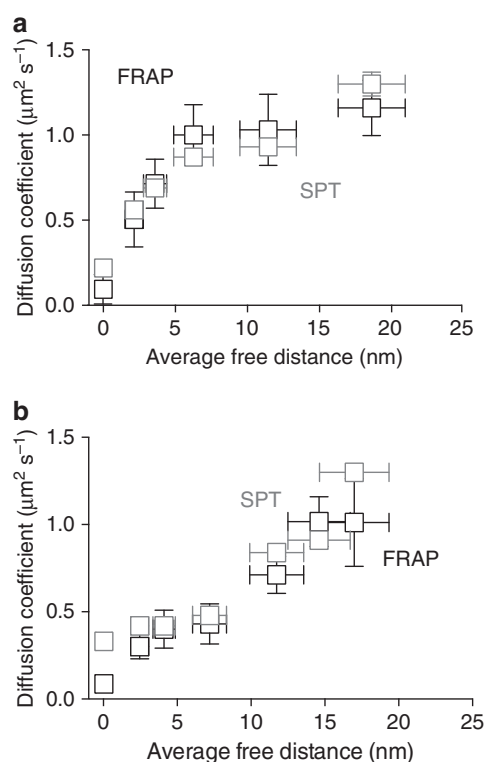


**Figure 5 | Comparison of VSG diffusion analysed by SPT or FRAP measurements.** The impact of the lateral protein density in supported membranes on the diffusion of wild type (a) or N-glycosylation deficient VSG121 (b) was analysed using SPT (grey squares) and FRAP (black squares). The error bars in y (diffusion coefficient) represent the standard deviation of the mean, while the error bars in x (average free distance) depict the range. SPT, single-particle tracking.

flasks with constant orbital shaking (80 r.p.m.). This cultivation procedure supports exponential growth of BSF to a maximum cell density of  $1 \times 10^7$  cells per ml.

**Purification and fluorescence labelling of membrane form VSG.** The purification of membrane form VSG (mfVSG) was carried out as published by Clarke *et al.*<sup>39</sup>. Cell pellets were washed three times in ice-cold TDB, proteins were extracted using a 0.1% trifluoroacetic acid solution on ice and subsequently purified via high-performance liquid chromatography. Purified mfVSG was labelled with ATTO 488 NHS-ester (DOL = 1 : 1 : 5 (v/v/v) 30% ammonia : 30% hydrogen peroxide : deionized-H<sub>2</sub>O for 30 min at 60 °C, followed by rigorous rinsing with deionized-H<sub>2</sub>O and drying at 70 °C. Hydrophilic glass cover slips were stored in a vacuum desiccator to avoid contamination with dust and were used within 2 days.

**Preparation of hydrophilic glass cover slips.** Glass cover slips (Hecht Assistant, No. 1, 24 mm diameter) were cleaned by sequential sonication in acetone, ethanol and methanol for 15 min each. After washing in deionized water the cover slips were soaked in a mixture of 1 : 1 : 5 (v/v/v) 30% ammonia : 30% hydrogen peroxide : deionized-H<sub>2</sub>O for 30 min at 60 °C, followed by rigorous rinsing with deionized-H<sub>2</sub>O and drying at 70 °C. Hydrophilic glass cover slips were stored in a vacuum desiccator to avoid contamination with dust and were used within 2 days.

**Incorporation of mfVSG into lipid bilayers.** Lipid bilayers were prepared from DOPE-biotin (1,2-dioleoyl-sn-glycero-3-phosphoethanolamine-N-cap-biotinyl) and/or SOPC (1-stearoyl-2-oleoyl-sn-glycero-3-phosphocholine, Avanti Polar Lipids Inc., Alabaster) by fusion of small unilamellar lipid vesicles on hydrophilic glass substrates (for details see Supplementary Methods section). Following preparation of the lipid bilayers, 0.2 nmol of fluorescently labelled mfVSG was applied to the sample chamber and incubated under light protection at 37 °C for 1 h. Finally, the sample was washed with 50 ml of vesicle buffer. For the preparation of heterogeneous protein layers, consisting of mfVSG and differing concentrations of NeutrAvidin (Invitrogen, Darmstadt), varying amounts of DOPE-biotin were added to the small unilamellar lipid vesicles (for details see Supplementary Methods section).

**mfVSG reconstitution and determination of lipid-to-protein ratio.** Labelled mfVSGs were reconstituted into liposomes by detergent extraction and subsequent removal of non-incorporated mfVSG by ultracentrifugation and dialysis<sup>47</sup> (for detailed information see Supplementary Methods section). Three aliquots of proteoliposomes were used in a modified total phosphorus assay (Anderson and Davis<sup>48</sup>; Bartlett<sup>49</sup>) to quantify the lipid concentration. The mfVSG concentration was determined photometrically and the lipid-to-protein ratio was calculated. The molar extinction coefficient of VSG at 280 nm was calculated by ProtParam based on the amino acid sequence of the mature VSG<sup>38</sup>.

SOPC monolayers were deposited on hydrophilic glass cover slips by Langmuir-Blodgett transfer using a Langmuir film balance (Kibron Inc., Finland). SOPC was dissolved in chloroform and spread on the water sub-phase of the Langmuir trough. The lipid monolayers were transferred to the glass cover slips at a constant surface pressure of 32 mN m<sup>-1</sup>.

The spacing of mfVSG on the artificial membranes was adjusted by diluting proteoliposomes of known lipid-to-protein ratio with defined amounts of protein-free liposomes. Pure or diluted proteoliposome samples were added to SOPC monolayers, incubated for 2 h at 37 °C and washed with 50 ml of vesicle buffer. For single-molecule microscopy experiments 0.1 pmol ATTO 647N-labelled mfVSG were then applied to preformed protein layers and incubated for 5–15 min at 37 °C. Finally, the samples were washed again with 50 ml of vesicle buffer.

**Absolute quantification of mfVSG in bilayers.** To determine the average free distance,  $d$ , between the VSG dimers the dimensions of the N-terminal domain of the known structures (VSG221 (PDB-ID: 1VSG) and ILTat1.24 (PDB-ID: 2VSG)) were measured at its greatest width (depth,  $d_{VSG}$ ) and smallest width (width,  $w_{VSG}$ ). With 6.5 nm, the largest value for  $d_{VSG}$  was found in VSG221 whereas ILTat1.24 displayed the smallest width with  $w_{VSG} = 4.5$  nm.

Using these dimensions, the average free distance,  $d$ , between VSG dimers within the SLB was calculated from the measured lipid-to-protein ratio,  $lpr$ , as follows:

$$d = \begin{cases} 2 \left( \frac{\sqrt{lpr \cdot A_L}}{\pi} \right) - r_{\text{rot}} & \text{if } lpr \geq 300 \\ (1-f) d_{lpr \leq 80} + f d_{lpr \geq 300} & \text{if } 80 < lpr < 300 \\ \frac{1}{2} \left( -(w_{VSG} - d_{VSG}) + \sqrt{(w_{VSG} - d_{VSG})^2 + 4A_L} \right) - l & \text{if } lpr \leq 80 \end{cases}, \quad (2)$$

where  $A_L = 0.6 \text{ nm}^2$  denotes the area per SOPC head group. At low protein densities ( $lpr \geq 300$ ) the VSG dimers were assumed to be able to rotate freely with  $r_{\text{rot}} = (d_{VSG}^2 + w_{VSG}^2)^{1/2}$  on a honeycomb lattice. The area of the rotating dimer is equivalent to  $\sim 80 \times A_L$ . In the limit of high protein densities ( $lpr \leq 80$ ) this rotation is assumed to be sterically impeded and the VSG dimers align on a

rectangular grid. This transition takes place at intermediate protein densities ( $80 < lpr < 300$ ). In this regime,  $d$  is calculated from the weighted mean of the two limiting cases. The weighting factor  $f = (lpr - 80)/219$ . The upper  $lpr$  threshold was chosen to ensure a smooth transition in the  $lpr$ -to- $d$  conversion.

**Relative quantification of mfVSG in proteoliposomes.** The density of mfVSG in artificial membranes was expressed as trypanosome cell surface equivalents. For this purpose, pure or diluted proteoliposome samples were added to SOPC monolayers and three aliquots of the supernatant were collected immediately or after 2 h of incubation at 37 °C. These two samples, A and B, were used to quantify the amount of mfVSG incorporated into the artificial membrane as explained in detail in Supplementary Methods section.

**Fluorescence microscopy and FRAP.** A fully automated inverted wide-field fluorescence microscope (TILL Photonics, Gräfelfing) was equipped with a Yanus digital scan head, 473 and 561 nm (Cobolt Inc., Solna) lasers, the appropriate emission and excitation filter cubes, Polychrome V (TILL Photonics) and a CCD camera (Sensicam, pixel size 6.4 μm, PCO, Kelheim). FRAP experiments were performed with a Nikon  $\times 60$  objective lens (NA 1.45). The laser was used for irreversible photobleaching of the region of interest. Polychrome V illumination was used to record pre and post-bleach frames. All equipment was controlled with the 'Live Acquisition' software (FEI) and images were analysed with the 'Offline Analysis' software packages (FEI). Protein diffusion was quantified by FRAP measurements. For measurements on living trypanosomes, line-FRAP was performed and data were analysed according to Phair *et al.*<sup>50</sup>. On artificial membranes circular regions of interest were bleached and diffusion was analysed according to Soumpasis *et al.*<sup>51</sup>.

**Analysis of lateral diffusion.** We calculated the frictional drag in artificial, supported membranes from the measured VSG diffusion coefficients in accordance with the approach of Evans and Sackmann which relates the diffusion coefficient  $D$  with the dimensionless radius  $\varepsilon$  (refs 10,15,52,53):

$$D = \frac{k_B T}{4\pi\eta_m} \left( \frac{1}{4} \varepsilon^2 + \frac{\varepsilon K_1(\varepsilon)}{K_0(\varepsilon)} \right), \quad (3)$$

where  $k_B$  is the Boltzmann constant,  $T$  the temperature and  $K_1$  and  $K_0$  modified Bessel functions of second kind with first or zeroth order, respectively.  $\eta_m$  is the membrane surface viscosity (bulk viscosity times membrane thickness).  $\varepsilon$  is given by

$$\varepsilon = R_p \sqrt{(b_s + b_\infty)/\eta_m}, \quad (4)$$

where  $R_p$  is the radius of the diffusing particle,  $b_s$  the friction coefficient with the substrate and  $b_\infty$  the friction coefficient with the ambient medium, either water or the VSG protein layer. In the dilute regime of low VSG concentrations the friction with the substrate is dominating over the friction with the ambient medium ( $b_s \gg b_\infty$ ). The opposite is true in the regime of high VSG concentrations. Thus,  $b_\infty$  can be determined from the diffusion coefficient measured at high VSG concentrations and the corresponding viscosity of the protein layer can be calculated according to

$$\mu_\infty = b_\infty \delta, \quad (5)$$

where  $\delta$  is a length which characterizes the penetration of the membrane flow field into the third dimension. Here, we assume that the membrane flow field will vanish over the full height of the protein layer, thus  $\delta = 15$  nm (refs 29,54).

Since equation (3) cannot be inverted easily, we employed a graphical solution to extract  $\varepsilon$  and subsequently calculated  $b$ . During the experiments the temperature was kept constant at  $T = 20$  °C. The relevant size of the diffusing particle in the membrane was determined by the two GPI anchors of the VSG dimer ( $R_p = 1$  nm). We use  $\eta_m = 0.65 \times 10^{-9}$  Pas. To make an educated guess of the 2D viscosity of a SOPC membrane at 20 °C, we linearly interpolated the reported values of DOPC at 10 °C ( $0.85 \times 10^{-9}$  Pas) and 45 °C ( $0.16 \times 10^{-9}$  Pas) (ref. 52). Comparison of this approximation with the known relationship between viscosity and temperature for water<sup>55</sup> and polymers<sup>56</sup> results in an error of less than 50% which does not influence the reported order of magnitude of the frictional coefficient.

**The effect of obstacles.** The diffusion in the presence of mobile obstacles was simulated by Saxton<sup>14</sup>, based on Tahir-Kheli<sup>12</sup> and van Beijeren *et al.*<sup>13</sup>,

$$\begin{aligned} D^*(A, \gamma) &= D(A, \gamma) = D(A)/D(0) = (1-A)f(A, \gamma), \\ f(A, \gamma) &= \frac{-[(1-\gamma)(1-A)f_0 + A] + \sqrt{[(1-\gamma)(1-A)f_0 + A]^2 + 4\gamma(1-A)f_0^2}}{2\gamma(1-A)f_0}, \\ f_0 &= (1-\alpha)/(1+\alpha(2\gamma-1)), \end{aligned} \quad (6)$$

where  $A$  is the area fraction of the obstacles and  $\alpha$  a lattice-specific constant ( $\alpha = 0.5$ , corresponding to a honeycomb lattice).  $\gamma$  is the ratio between the jump rate of a diffusing particle and the jump rate of obstacles. We chose this model to analyse the diffusion of VSG in the presence and absence of NeutrAvidin. In our



experiments, we interpret the measured immobile VSG fraction as the area fraction of mobile obstacles. It should be noted, that the immobile fraction is only immobile on the timescales used for the experiment not, however, at longer timescales. Thus, the VSG is tracer and obstacle at the same time while NeutrAvidin is only a modulating factor without an explicit analogue in the model. The fit is presented in a plot of the mobile fraction  $mf$  versus  $D/D_0$  (see Fig. 3). To this end, the data of the immobile fraction  $imf$  are converted via  $mf = 1 - imf$ .

**Single-molecule tracking.** Image analysis was done as described before<sup>57,58</sup> using programs written in MatLab (Mathworks Inc., USA). In brief, each frame of a single-molecule movie was corrected for static background by low-spatial frequency filtering. The  $x/y$  positions of the individual ATTO 647N molecules were determined by fitting a 2D-Gaussian to the acquired intensity distributions. This data set was further filtered by comparison to the single-molecule footprint of ATTO 647N (intensity, width) and detection error thresholds. Trajectories were obtained from the single-molecule positions using a probabilistic algorithm that calculates the probability of a particle with diffusion coefficient  $D_{in}$  to reappear at a different position in the subsequent frame. A transitional matrix is built up, which includes the probabilities of all possible connections between all molecules in neighbouring frames. From these a combination of connections is chosen in such a way that the total probability is maximized. For more details on how to choose  $D_{in}$  properly, see the Supplementary Methods section and the Supplementary Fig. 5.

Only trajectories with 20 or more steps were analysed further. They were categorized as mobile or immobile by comparison with the achieved localization precision,  $\sigma$ . An immobile particle is characterized by  $msd_{immob} = 4\sigma^2$ .

Starting from the trajectories of mobile particles, the mean squared displacement,  $msd$ , was calculated as a function of time,  $t$ . Both the  $msd$  and the time between frames were subsequently corrected for limitations in the time and spatial resolution<sup>25,59,60</sup>.

$$msd_{corr} = msd - 4\sigma^2 \text{ and } t_{corr} = t - \frac{t_{ill}}{3}, \quad (7)$$

where  $t_{ill}$  denotes the illumination time.  $D_{out}$  was calculated as one-fourth of the slope of the  $msd_{corr}(t_{corr})$  curve resulting from a linear fit to the five first data points.

**Data availability.** All the relevant data that support the findings of this study are in principle available from the corresponding author upon request.

## References

- Saffman, P. G. & Delbrück, M. Brownian motion in biological membranes. *Proc. Natl Acad. Sci. USA* **72**, 3111–3113 (1975).
- Peters, R. & Cherry, R. J. Lateral and rotational diffusion of bacteriorhodopsin in lipid bilayers: experimental test of the Saffman-Delbrück equations. *Proc. Natl Acad. Sci. USA* **79**, 4317–4321 (1982).
- Lee, C. C., Revington, M., Dunn, S. D. & Petersen, N. O. The lateral diffusion of selectively aggregated peptides in giant unilamellar vesicles. *Biophys. J.* **84**, 1756–1764 (2003).
- Cicuta, P., Keller, S. L. & Veatch, S. L. Diffusion of liquid domains in lipid bilayer membranes. *J. Phys. Chem. B* **111**, 3328–3331 (2007).
- Ramadurai, S. *et al.* Lateral diffusion of membrane proteins. *J. Am. Chem. Soc.* **131**, 12650–12656 (2009).
- Weiß, K. *et al.* Quantifying the diffusion of membrane proteins and peptides in black lipid membranes with 2-focus fluorescence correlation spectroscopy. *Biophys. J.* **105**, 455–462 (2013).
- Fenz, S. F., Sachse, R., Schmidt, T. & Kubick, S. Cell-free synthesis of membrane proteins: tailored cell models out of microsomes. *Biochim. Biophys. Acta* **1838**, 1382–1388 (2014).
- Hughes, B. D., Shlesinger, M. F. & Montroll, E. W. Random walks with self-similar clusters. *Proc. Natl Acad. Sci. USA* **78**, 3287–3291 (1981).
- Petrov, E. P. & Schwille, P. Translational diffusion in lipid membranes beyond the Saffman-Delbrück approximation. *Biophys. J.* **94**, L41–L43 (2008).
- Evans, E. & Sackmann, E. Translational and rotational drag coefficients for a disk moving in a liquid membrane associated with a rigid substrate. *J. Fluid Mech.* **194**, 553–561 (1988).
- Engelman, D. M. Membranes are more mosaic than fluid. *Nature* **438**, 578–580 (2005).
- Tahir-Kheli, R. Tracer diffusion at the percolation threshold. *Phys. Rev. B* **32**, 3604–3606 (1985).
- van Beijeren, H., Kutner, R. & Kehr, K. Tracer diffusion on two coupled lines: the long-time tail of the velocity autocorrelation function compared to the mode-coupling prediction. *Phys. Rev. B* **32**, 466–467 (1985).
- Saxton, M. J. Lateral diffusion in an archipelago. The effect of mobile obstacles. *Biophys. J.* **52**, 989–997 (1987).
- Fenz, S. F., Merkel, R. & Sengupta, K. Diffusion and intermembrane distance: case study of avidin and E-cadherin mediated adhesion. *Langmuir* **25**, 1074–1085 (2009).
- Casuso, I. *et al.* Characterization of the motion of membrane proteins using high-speed atomic force microscopy. *Nat. Nanotechnol.* **7**, 525–529 (2012).
- Horton, M. R., Hoefling, F., Raedler, J. O. & Franosch, T. Development of anomalous diffusion among crowding proteins. *Soft Matter* **6**, 2648–2656 (2010).
- Frick, M., Schmidt, K. & Nichols, B. J. Modulation of lateral diffusion in the plasma membrane by protein density. *Curr. Biol.* **17**, 462–467 (2007).
- Rassam, P. *et al.* Supramolecular assemblies underpin turnover of outer membrane proteins in bacteria. *Nature* **523**, 333–336 (2015).
- Domański, J., Marrink, S. J. & Schäfer, L. V. Transmembrane helices can induce domain formation in crowded model membranes. *Biochim. Biophys. Acta* **1818**, 984–994 (2012).
- Goose, J. E. & Sansom, M. S. P. Reduced lateral mobility of lipids and proteins in crowded membranes. *PLoS Comput. Biol.* **9**, e1003033 (2013).
- Javanainen, M., Monticelli, L., la Serna, de, J. B. & Vattulainen, I. Free volume theory applied to lateral diffusion in langmuir monolayers: atomistic simulations for a protein-free model of lung surfactant. *Langmuir* **26**, 15436–15444 (2010).
- Guigas, G. & Weiss, M. Effects of protein crowding on membrane systems. *Biochim. Biophys. Acta* **107**, 407–427 (2015).
- Zhang, F. *et al.* Lateral diffusion of membrane-spanning and glycosylphosphatidylinositol-linked proteins: toward establishing rules governing the lateral mobility of membrane proteins. *J. Cell Biol.* **115**, 75–84 (1991).
- Wieser, S., Moertelmaier, M., Fuerstbauer, E., Stockinger, H. & Schütz, G. J. (Un)confined diffusion of CD59 in the plasma membrane determined by high-resolution single molecule microscopy. *Biophys. J.* **92**, 3719–3728 (2007).
- Pinaud, F. *et al.* Dynamic partitioning of a glycosyl-phosphatidylinositol-anchored protein in glycosphingolipid-rich microdomains imaged by single-quantum dot tracking. *Traffic* **10**, 691–712 (2009).
- Hartel, A. J. W. *et al.* The molecular size of the extra-membrane domain influences the diffusion of the GPI-anchored VSG on the trypanosome plasma membrane. *Sci. Rep.* **5**, 10394 (2015).
- Grünfelder, C. G. *et al.* Endocytosis of a glycosylphosphatidylinositol-anchored protein via clathrin-coated vesicles, sorting by default in endosomes, and exocytosis via RAB11-positive carriers. *Mol. Biol. Cell.* **14**, 2029–2040 (2003).
- Vickerman, K. & Luckins, A. G. Localization of variable antigens in the surface coat of *Trypanosoma brucei* using ferritin conjugated antibody. *Nature* **224**, 1125–1126 (1969).
- Cross, G. A. Identification, purification and properties of clone-specific glycoprotein antigens constituting the surface coat of *Trypanosoma brucei*. *Parasitology* **71**, 393–417 (1975).
- Cross, G. A. Antigenic variation in trypanosomes: secrets surface slowly. *Bioessays* **18**, 283–291 (1996).
- Blum, M. L. *et al.* A structural motif in the variant surface glycoproteins of *Trypanosoma brucei*. *Nature* **362**, 603–609 (1993).
- Jones, N. G. *et al.* Structure of a glycosylphosphatidylinositol-anchored domain from a trypanosome variant surface glycoprotein. *J. Biol. Chem.* **283**, 3584–3593 (2008).
- Ferguson, M. A., Low, M. G. & Cross, G. A. Glycosyl-sn-1,2-dimyristylphosphatidylinositol is covalently linked to *Trypanosoma brucei* variant surface glycoprotein. *J. Biol. Chem.* **260**, 14547–14555 (1985).
- Mehlert, A., Zitzmann, N., Richardson, J. M., Treumann, A. & Ferguson, M. A. The glycosylation of the variant surface glycoproteins and procyclic acidic repetitive proteins of *Trypanosoma brucei*. *Mol. Biochem. Parasitol.* **91**, 145–152 (1998).
- Heddergott, N. *et al.* Trypanosome motion represents an adaptation to the crowded environment of the vertebrate bloodstream. *PLoS Pathog.* **8**, e1003023 (2012).
- Bülow, R., Overath, P. & Davoust, J. Rapid lateral diffusion of the variant surface glycoprotein in the coat of *Trypanosoma brucei*. *Biochemistry* **27**, 2384–2388 (1988).
- Carrington, M. *et al.* Variant specific glycoprotein of *Trypanosoma brucei* consists of two domains each having an independently conserved pattern of cysteine residues. *J. Mol. Biol.* **221**, 823–835 (1991).
- Clarke, M. W., Olafson, R. W. & Pearson, T. W. Rapid preparative scale purification of myristylated variant surface glycoproteins from African trypanosomes. *Mol. Biochem. Parasitol.* **17**, 19–34 (1985).
- Schubert, T., Seitz, P. & Schneck, E. Structure of synthetic transmembrane lipid membranes at the solid/liquid interface studied by X-ray reflectivity. *J. Phys. Chem.* **112**, 10041–10044 (2008).
- Guigas, G. & Weiss, M. Size-dependent diffusion of membrane inclusions. *Biophys. J.* **91**, 2393–2398 (2006).
- Engstler, M. *et al.* Hydrodynamic flow-mediated protein sorting on the cell surface of trypanosomes. *Cell* **131**, 505–515 (2007).
- Hoiberg-Nielsen, R., Westh, P., Skov, L. K. & Arleth, L. Interrelationship of steric stabilization and self-crowding of a glycosylated protein. *Biophys. J.* **97**, 1445–1453 (2009).
- Wirtz, E., Leal, S., Ochatt, C. & Cross, G. A. A tightly regulated inducible expression system for conditional gene knock-outs and dominant-negative genetics in *Trypanosoma brucei*. *Mol. Biochem. Parasitol.* **99**, 89–101 (1999).

45. Muñoz-Jordán, J. L., Davies, K. P. & Cross, G. A. Stable expression of mosaic coats of variant surface glycoproteins in *Trypanosoma brucei*. *Science* **272**, 1795–1796 (1996).
46. Grünfelder, C. G. *et al.* Accumulation of a GPI-anchored protein at the cell surface requires sorting at multiple intracellular levels. *Traffic* **3**, 547–559 (2002).
47. Erb, E. M., Tangemann, K., Bohrmann, B., Müller, B. & Engel, J. Integrin  $\alpha$ IIb  $\beta$ 3 reconstituted into lipid bilayers is nonclustered in its activated state but clusters after fibrinogen binding. *Biochemistry* **36**, 7395–7402 (1997).
48. Anderson, R. L. & Davis, S. An organic phosphorus assay which avoids the use of hazardous perchloric acid. *Clin. Chim. Acta* **121**, 111–116 (1982).
49. Bartlett, G. Phosphorus assay in column chromatography. *J. Biol. Chem.* **234**, 466–468 (1959).
50. Phair, R. & Misteli, T. Kinetic modelling approaches to *in vivo* imaging. *Nat. Rev. Mol. Cell. Biol.* **2**, 898–907 (2001).
51. Soumpasis, D. M. Theoretical analysis of fluorescence photobleaching recovery experiments. *Biophys. J.* **41**, 95–97 (1983).
52. Merkel, R., Sackmann, E. & Evans, E. Molecular friction and epitactic coupling between monolayers in supported bilayers. *J. Phys. France* **50**, 1535–1555 (1989).
53. Purucker, O., Förtig, A., Jordan, R., Sackmann, E. & Tanaka, M. Control of frictional coupling of transmembrane cell receptors in model cell membranes with linear polymer spacers. *Phys. Rev. Lett.* **98**, 078102 (2007).
54. Abuillan, W. *Fine-Structures, Lateral Correlation and Diffusion of Membrane-Associated Proteins on Biological Membrane Surfaces*. PhD thesis (University of Heidelberg, 2013).
55. Al-Shemmeri, T. T. *Engineering Fluid Mechanics Solution Manual* (Ventus Publishing, 2012).
56. Williams, M. L., Landel, R. F. & Ferry, J. D. The temperature dependence of relaxation mechanisms in amorphous polymers and other glass-forming liquids. *J. Am. Chem. Soc.* **77**, 3701–3707 (1955).
57. Schmidt, T., Schütz, G. J., Baumgartner, W., Gruber, H. J. & Schindler, H. Imaging of single molecule diffusion. *Proc. Natl Acad. Sci. USA* **93**, 2926–2929 (1996).
58. Fenz, S., Pezzarossa, A. & Schmidt, T. *The Basics and Potential of Single-Molecule Tracking in Cellular Biophysics, Comprehensive Biophysics Vol 2* (ed. Egelman, Edward H.) (Academic Press, 2012).
59. Schmidt, T. & Schütz, G. J. *Handbook of Single Molecule Biophysics* (Springer-Verlag 19–42, 2009).
60. Semrau, S., Pezzarossa, A. & Schmidt, T. Microsecond single-molecule tracking ( $\mu$ SMT). *Biophys. J.* **100**, L19–L21 (2011).

## Acknowledgements

M.E. is indebted to Peter Overath for expert discussion. This work was supported by the Deutsche Forschungsgemeinschaft (grants EN 305 and GRK 1114 to M.E.) and the Sonderforschungsbereich 630. M.E. is a member of the Wilhelm Conrad Röntgen-Center for Complex Material Systems (RCCM). M.T. thanks the German Science Foundation (GRK 1164 and SFB 873 for support). M.T. is a member of the German Excellence Cluster 'Cell Network'. The iCeMS is supported by World Premier International Research Center Initiative (WPI), MEXT, Japan. We thank R. Merkel (Jülich) for useful advice concerning the extraction of the viscosity of the VSG protein layer. We are grateful to T. Schmidt (Leiden) for single-molecule data analysis tools.

## Author contributions

M.E., A.J.W.H., N.G.J., M.G., S.F.F. and M.T. designed research. M.E., A.J.W.H., M.G., C.B. A.H., N.G.J., W.A. performed the research. A.J.W.H., M.G., C.B., M.E., S.F.F., N.G.J., W.A. and M.T. analysed the data. A.J.W.H., M.G., N.G.J., S.F.F. and M.E. wrote the paper.

## Additional information

**Supplementary Information** accompanies this paper at <http://www.nature.com/naturecommunications>

**Competing financial interests:** The authors declare no conflict of interests.

**Reprints and permission** information is available online at <http://npg.nature.com/reprintsandpermissions/>

**How to cite this article:** Hartel, A. J. W. *et al.* N-glycosylation enables high lateral mobility of GPI-anchored proteins at a molecular crowding threshold. *Nat. Commun.* 7:12870 doi: 10.1038/ncomms12870 (2016).



This work is licensed under a Creative Commons Attribution 4.0 International License. The images or other third party material in this article are included in the article's Creative Commons license, unless indicated otherwise in the credit line; if the material is not included under the Creative Commons license, users will need to obtain permission from the license holder to reproduce the material. To view a copy of this license, visit <http://creativecommons.org/licenses/by/4.0/>

© The Author(s) 2016